

## First Proton-Proton Physics with the ALICE detector

---

**Jan Fiete GROSSE-OETRINGHAUS**\*†

*CERN, Geneva and Institut fuer Kernphysik, Muenster*

*E-mail: jan.fiete.grosse-oetringhaus@cern.ch*

This paper describes the status and plans of first measurements in p+p collisions with ALICE. The first part introduces the ALICE experiment with a focus on the subdetectors that are to be used for first physics. The characteristic features of ALICE, its very low-momentum cut-off, the low material budget and the excellent PID and vertexing capabilities, that make ALICE an important contributor to LHC physics in the realm of soft QCD, are described. Subsequently, a selection of measurements that are accessible with data taken in a few days to 1–2 weeks are discussed: the pseudorapidity density  $dN_{ch}/d\eta$ , the multiplicity distribution and the transverse momentum distribution  $dN_{ch}/dp_T$  of charged particles.

*Physics at LHC 2008*

*29 September - October 4, 2008*

*Split, Croatia*

---

\*Speaker.

†for the ALICE collaboration

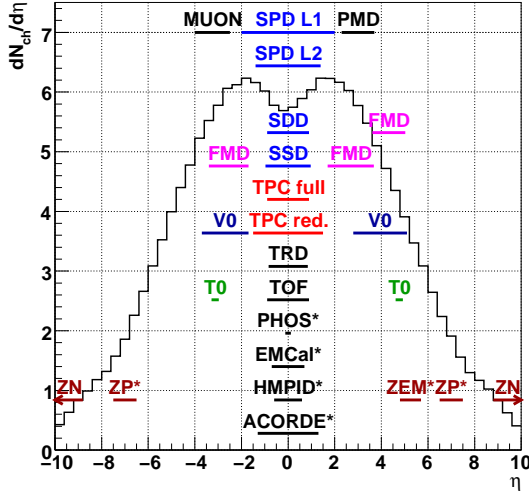


**Figure 1:** Acceptance in  $\eta$  of the subdetectors overlaid with a  $dN_{ch}/d\eta$  prediction by Pythia. The subdetectors have full coverage in azimuth except the ones marked with an asterisk. Two ranges are given for the TPC, depending if full or reduced track length is required. For more details see [1].

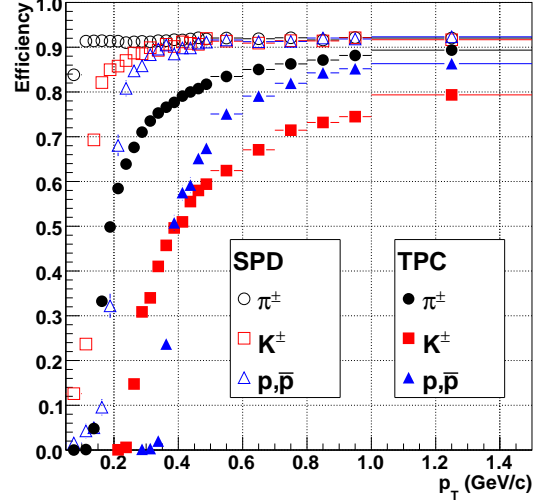


**Figure 2:** Physical efficiency to track primary particles in the SPD (open symbols) and the TPC (closed symbols) as function of  $p_T$ , separately for pions, kaons and protons. The larger energy loss for protons and kaons compared to pions reduces the efficiency at low  $p_T$ . Furthermore, kaon decays occur at low  $p_T$  inside the tracking volume.

## 1. ALICE

A Large Ion Collider Experiment (ALICE) [1] is a general-purpose particle detector designed to study heavy-ion collisions at the LHC. The detector's unique features are tracking and particle identification over a large range of momenta, from tens of MeV/c to over 100 GeV/c, therefore accessing topics starting from soft physics to jets and high- $p_T$  particle production. In ALICE it is possible to reconstruct the primary vertex and secondary vertices of e.g. hyperons and heavy quark mesons with a resolution better than 100  $\mu\text{m}$ .

The detector consists of a central barrel ( $|\eta| < 0.9$ ) optimized for the detection of hadrons, electrons and photons, a muon spectrometer at forward rapidities as well as additional forward and trigger detectors. The central barrel is contained in a magnetic field of up to 0.5 T. Figure 1 shows the coverage in pseudorapidity  $\eta = -\ln \tan \theta/2$  ( $\theta$  being the angle w.r.t. the beam axis) of the various subdetectors. Besides the heavy-ion program where ALICE will take data mostly in Pb+Pb collisions with up to  $\sqrt{s_{NN}} = 5.5 \text{ TeV}$ , the study of p+p collisions (up to  $\sqrt{s} = 14 \text{ TeV}$ ) is an integral part of the physics program.

### 1.1 Silicon Pixel Detector (SPD)

The first two layers of the Inner Tracking System (ITS), called Silicon Pixel Detector (SPD), that are placed at a radial distance of 3.9 cm and 7.6 cm from the beam line, are based on hybrid silicon pixels. These allow measurements in an environment of up to 50 particles per  $\text{cm}^2$  in Pb+Pb collisions and still retain an occupancy of only a few percent. The SPD allows to access the

multiplicity with a low-momentum cut-off of about 35 MeV/c at 0.5 T field. Particles in  $|\eta| < 1.4$  emerging from collisions at the nominal interaction-point leave hits in both layers. However, the spread of the  $z$  vertex position allows to measure the  $dN_{ch}/d\eta$  distribution up to  $\eta \approx \pm 2.0$ . The pixels themselves have an efficiency of above 99%. However, at present (November 2008) about 10% of the detector need a hardware intervention that will be partly addressed in the upcoming shutdown period. The tracking efficiency for different particle species is shown in Figure 2.

Each of the SPD's 1200 chips provides a so-called *fast OR* signal which indicates if at least one signal was detected in the given chip. This is used for the minimum bias trigger and allows to trigger on high-multiplicity events.

The SPD modules have been realigned using 50,000 cosmic muons tracks. The comparison of the reconstructed upper and lower half of a traversing cosmic muon allows to estimate the effect of the residual misalignment which amounts to less than 10  $\mu\text{m}$  in  $r\phi$  direction.

## 1.2 Time Projection Chamber (TPC)

ALICE's Time Projection Chamber (TPC) is the largest in the world, it spans between 0.85 m and 2.5 m in radial direction and has a length of 5 m. It allows to measure up to 160 clusters per track in  $|\eta| < 0.9$  which results in an excellent track resolution and particle identification without being affected by the Landau tail in the energy-loss distribution. The tracking efficiency for different particle species is shown in Figure 2. The low-momentum cut-off is about 200 MeV/c for pions and larger for other particle species. A track that traverses ITS and TPC sees only about 10% of a radiation length.

## 1.3 Minimum Bias Trigger

ALICE's minimum bias trigger is based on the signals from the V0 detector that consists out of two arrays of segmented scintillator counters. The time resolution is of the order of 1 ns [2] which allows to identify beam-gas events that occurred outside of the nominal interaction region. The V0 provides three trigger bits, one for each side of the detector (V0\_L and V0\_R) and the beam-gas detection bit (V0\_BG). Furthermore, the SPD provides a trigger bit which requires at least one hit in the SPD (SPD\_OR). These inputs are combined to the following triggers:

- MB1 = (V0\_L or V0\_R or SPD\_OR) and !V0\_BG;
- MB2 = (V0\_L or V0\_R) and SPD\_OR and !V0\_BG;
- MB3 = V0\_L and V0\_R and SPD\_OR and !V0\_BG.

Based on cross sections predicted by Pythia [3] and the full detector simulation, the MB1 trigger is evaluated to be sensitive to 90.3% (88.6%) of the inelastic cross section at 14 TeV (900 GeV), respectively. For non single-diffractive (NSD) events the sensitivity is 96.3% (95.0%) at 14 TeV (900 GeV), respectively.

However, for first measurements these triggers are not used during data-taking, but for the event selection in the analysis. Instead a bunch-crossing trigger will be used that allows to evaluate the trigger performance. Furthermore, a trigger on single bunches allows to estimate the effect of beam-gas events.

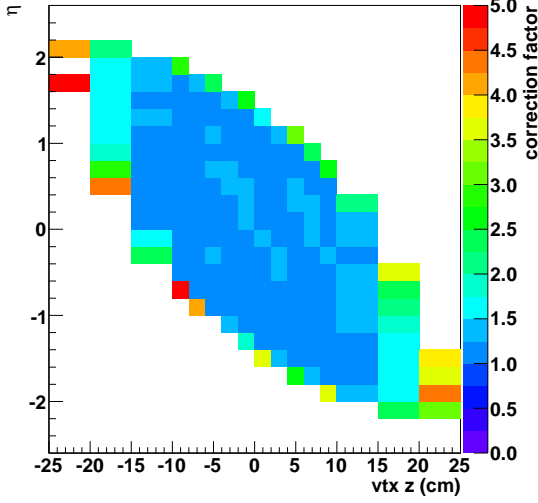


**Figure 3:** Tracking efficiency and acceptance correction for the SPD. The dependence of the acceptance on the vertex position can be clearly seen. In the white area the correction is larger than 5.

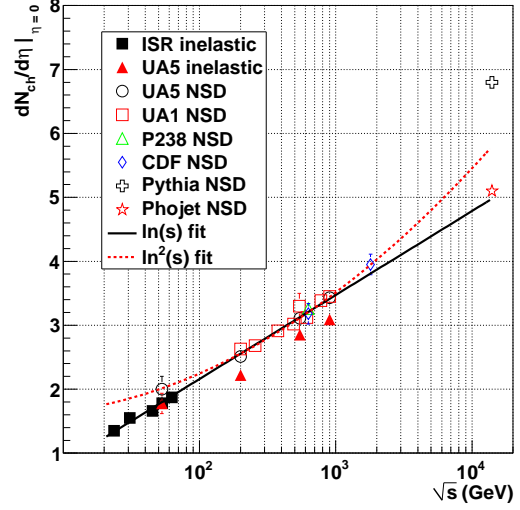


**Figure 4:**  $dN_{ch}/d\eta|_{\eta=0}$  as function of  $\sqrt{s}$  [3, 4, 5, 6, 7]. Only NSD data is used for the fits.

## 2. First Measurements

The measurements described in the following have the aim of characterizing LHC collisions and studying the energy dependence of the observables. The understanding of the realm of soft QCD will allow to tune Monte Carlo (MC) generators in the new energy regime. A good knowledge of the underlying event is fundamental for the analysis of rare signals and a required baseline for the upcoming Pb+Pb measurements in ALICE.

### 2.1 Pseudorapidity Density $dN_{ch}/d\eta$

The measurement of the pseudorapidity density is performed with the SPD. It can also be done with the TPC which allows a cross check in the overlapping phase space region. About 20,000 – 40,000 events are sufficient for this analysis.

$dN_{ch}/d\eta$  is calculated by counting the number of tracks ( $T$ ) in a given  $\eta$ -bin ( $d\eta$ ) and normalizing with the number of events ( $E$ ), taking into account a set of corrections  $C$ :  $dN_{ch}/d\eta = T/E \times C$ . The correction for acceptance, tracking efficiency and low-momentum cut-off is shown in Figure 3 in the  $\eta$  vs. vtx- $z$  ( $z$  position of the vertex) plane. This correction also includes effects of secondaries, decay and stopping of particles. Furthermore, the efficiency of the vertex reconstruction and the trigger bias has to be corrected for. Collisions occurring at large  $|\text{vtx-}z|$  can be used to extend the  $\eta$ -range, however, the normalization ( $E$ ) becomes  $\eta$ -dependent.

Figure 4 shows  $dN_{ch}/d\eta|_{\eta=0}$  as function of  $\sqrt{s}$  from ISR to Tevatron energies. The NSD data is fitted using a  $\ln s$ - and  $\ln^2 s$ -dependent function which allows an extrapolation to  $\sqrt{s} = 14$  TeV. The predictions by Pythia and Phojet [4] are also shown.

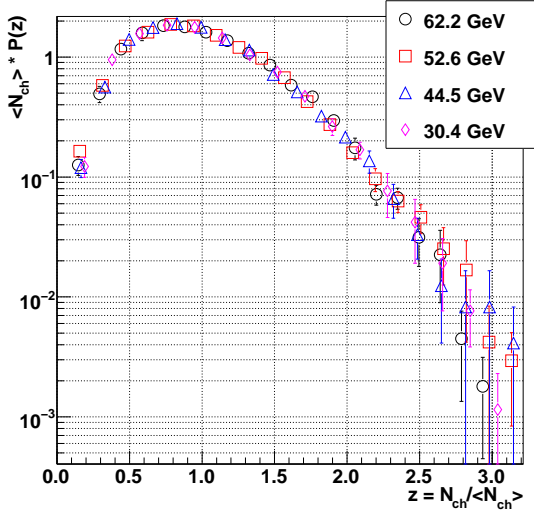


**Figure 5:** Normalized multiplicity distributions by ISR for NSD events in full phase space [8] in KNO variables.

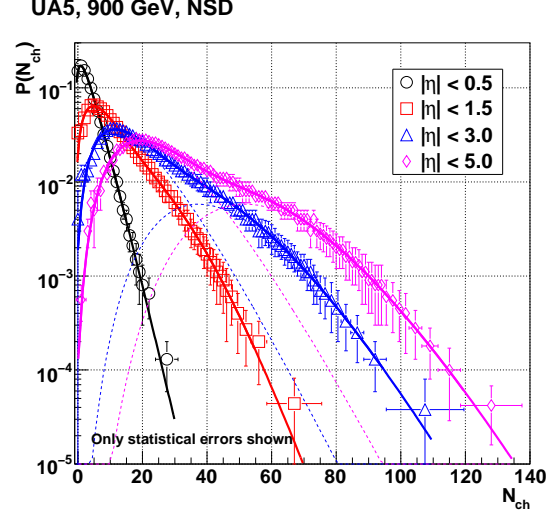


**Figure 6:** Normalized multiplicity distributions in various rapidity intervals [7] fitted with a combination of two NBDs. The two contributing NBDs (dashed lines) are shown for  $|\eta| < 3.0$  and  $5.0$ .

A full set of systematic studies has been performed including the evaluation of uncertainties in the particle composition and cross sections as well as the material budget. The effects of the track selection cuts, low-momentum cut-off and misalignment has been studied. Only the uncertainties on the relative cross sections of the different process types (non-diffractive (ND), single-diffractive (SD) and double-diffractive (DD)) give a non-negligible contribution to the systematic error. Varying the relative cross sections (ND/SD, ND/DD) by up to 50% results in a systematic error of 2% for the correction to the full inelastic cross section and 8% to the non-single-diffractive cross section. Other contributions to the systematic uncertainty may come from miscalibration, beam-gas and pileup. Their magnitude will have to be judged depending on the running conditions at data-taking.

## 2.2 Charged Particle Multiplicity Distribution

The measurement of the multiplicity distribution is performed with the SPD. The same statistics of 20,000 – 40,000 events are sufficient to obtain a distribution that reaches up to  $\approx 5$  times the mean multiplicity.

The charged particle multiplicity distribution, the probability  $P(N_{ch})$  to find an event with multiplicity  $N_{ch}$ , can be described over a broad range in energy by KNO scaling [9] which means that all multiplicity distributions fall onto one curve when expressed as function of  $z = N_{ch} / \langle N_{ch} \rangle$ . Data from ISR that follows KNO scaling is shown in Figure 5. This scaling is found to be broken at Sp $\bar{p}$ S energies [10], first for full phase space, at higher energies also in limited  $\eta$ -intervals. Negative binomial distributions (NBDs) [6] describe the data at higher energies better. At 1.8 TeV, however, only the multiplicity distribution in a very central region ( $|\eta| < 0.5$ ) follows a NBD [11].

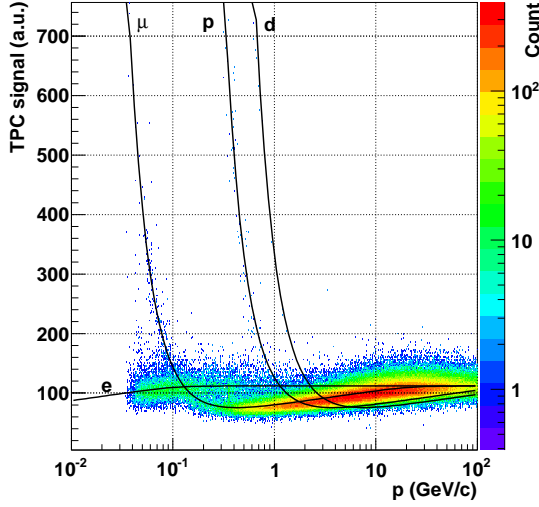


**Figure 7:** Energy loss in the TPC of about 5 million cosmic tracks fitted with parameterizations (Figure from [12]).

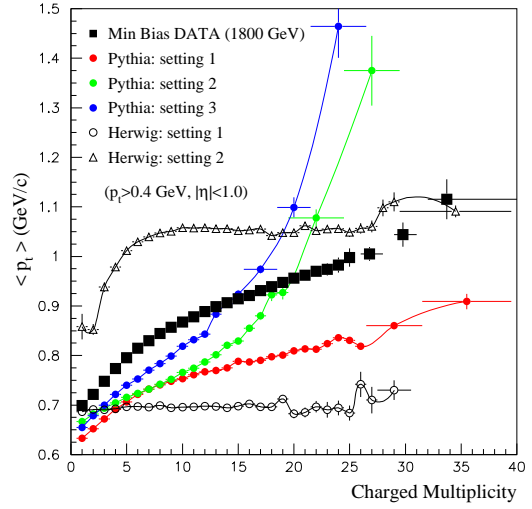


**Figure 8:**  $\langle p_T \rangle$  vs. charged multiplicity measured by CDF. Black squares are data points, the other curves are predictions by Pythia and Herwig with different tunes. Note that none of them reproduces the data (Figure from [13]).

The two component model [14] combines two NBD-shaped components, a soft and a semihard one. Data from UA5 fitted with this approach is shown in Figure 6.

The steeply falling multiplicity spectrum necessitates to unfold the measured data. This allows to produce the multiplicity distribution unaffected by bin flow and independent of the MC input distribution that has been used to gain the detector's response. It is recalled that Pythia and Phojet have a significantly different prediction for the multiplicity distribution at  $\sqrt{s} = 14 \text{ TeV}$  (see e.g. [15]). Two unfolding methods have been prepared for the analysis, a method based on  $\chi^2$  minimization and one based on Bayes' theorem [16]. Both perform well and will be used to obtain the charged particle multiplicity distribution from first data. More information including the performed systematic studies can be found in [17].

### 2.3 Transverse Momentum Distribution $dN_{ch}/dp_T$

The unidentified  $p_T$  spectrum from  $\approx 200 \text{ MeV}/c$  up to a  $p_T$  of  $20 \text{ GeV}/c$  can be obtained from a sample of about 150,000 events using the TPC.

The TPC has a built-in laser system that allows to perform sufficient alignment and calibration already before the start of data taking. However, already without calibration the  $p_T$  resolution is satisfactory for first measurements. The  $p_T$  resolution was obtained by comparing the reconstructed upper and lower half of traversing cosmic muons; it is about 2% at  $p_T = 2 \text{ GeV}/c$  increasing to 10% at  $10 \text{ GeV}/c$ .

Identified  $p_T$  spectra in the region up to  $1 \text{ GeV}/c$  can be obtained from 20,000 – 40,000 events. The TPC PID has been calibrated with Krypton and yields a  $dE/dx$  resolution of about 5.7% [12].

Figure 7 shows the energy loss of tracks from cosmic rays and their interactions as function of their momentum.

Furthermore, it is interesting to study the correlation  $\langle p_T \rangle$  vs.  $N_{ch}$ , the balance between particle production and transverse energy. Figure 8 shows this quantity measured by CDF at  $\sqrt{s} = 1.8$  TeV. Its behavior has not yet been satisfactorily explained by models or event generators.

### 3. Summary

ALICE can measure within a few days to 1–2 weeks of data-taking basic properties of p+p collisions from 900 GeV to 14 TeV. The measurements in this period will allow to access the phase space around mid-rapidity ( $|\eta| < 2.0$ ) from a very low momentum of about 35 MeV/c to about 20 GeV/c. Furthermore, particle identification is available over a large momentum range. These measurements allow to characterize the underlying event, tune MC generators and in consequence open the door for the study of rare signals and heavy-ion collisions.

The outlined topics compose only the very first measurements available with ALICE. Other interesting topics that will be addressed in p+p collisions are baryon transport, strangeness and resonance production, femtoscopy, the study of heavy flavor and jets, and many more.

### References

- [1] K. Aamodt *et al.*, JINST **3** (2008) S08002.
- [2] F. Carminati *et al.*, J. Phys. G **30** (2004) 1517.
- [3] T. Sjostrand *et al.*, Comput. Phys. Commun. 135 (2001) 238; V6.214 with “ATLAS tune” [15].
- [4] R. Engel and J. Ranft, Phys. Rev. D **54** (1996) 4244
- [5] W. Thome *et al.* Nucl. Phys. B **129** (1977) 365; F. Abe *et al.*, Phys. Rev. D **41** (1990) 2330; C. Albajar *et al.*, Nucl. Phys. B **335** (1990) 261.
- [6] G. J. Alner *et al.*, Phys. Lett. B **160** (1985) 193.
- [7] R. E. Ansorge *et al.*, Z. Phys. C **43** (1989) 357.
- [8] A. Breakstone *et al.* Phys. Rev. D **30** (1984) 528.
- [9] Z. Koba, H. B. Nielsen and P. Olesen, Nucl. Phys. B **40** (1972) 317.
- [10] G. J. Alner *et al.*, Phys. Lett. B **167** (1986) 476.
- [11] F. Rimondi, Aspen Multipart. Dyn. 1993:0400-404.
- [12] A. Kalweit, GSI and Technical University Darmstadt, Private Communication.
- [13] D. E. Acosta *et al.*, Phys. Rev. D **65** (2002) 072005.
- [14] A. Giovannini and R. Ugoccioni, Phys. Rev. D **59** (1999) 094020.
- [15] A. Moraes, C. Buttar and I. Dawson, Eur. Phys. J. C **50** (2007) 435.
- [16] G. D’Agostini, Nucl. Instrum. Meth. A **362** (1995) 487.
- [17] J. F. Grosse-Oetringhaus, ALICE-INT-2008-002 (2008).